The Effect of Zero-Point Energy in Simulating Organic Reactions with Post-Transition State Bifurcation

Matthew T. Tremblay,[1] *Zhongyue J. Yang*[1-4,*]

[1]Department of Chemistry, Vanderbilt University, Nashville, Tennessee 37235, United States. [2]Center for Structural Biology, Vanderbilt University, Nashville, Tennessee 37235, United States. [3]Vanderbilt Institute of Chemical Biology, Vanderbilt University, Nashville, Tennessee 37235, United States. [4]Data Science Institute, Vanderbilt University, Nashville, Tennessee 37235, United States

Corresponding Authors

Zhongyue John Yang – email: zhongyue.yang@vanderbilt.edu phone: 615-343-9849

ABSTRACT: Ambimodal reactions involve a single transition state leading to multiple products. To assess the ratio of the bifurcation products, quasiclassical trajectories (QCTs) are initiated from transition state geometries that are randomly sampled using the zero-point energy (ZPE) plus thermal energy of a molecule's vibrational modes. However, in the QCTs, the influence of ZPE percentage in the resulting bifurcation ratio and time gap between formation of bonds is not well understood. To benchmark the effect of varying the percentage of the molecules' inherent ZPE used in the simulation, three organic reactions with distinct mechanisms that all display post-transition state bifurcation were selected. The three reactions studied include an intramolecular [6+4]/[4+2] cycloaddition, an asynchronous nitrene insertion, and an S_N2/addition to a carbonyl on an α-bromoketone. These reactions encompass various modes of bond formation and cleavage, offering a broad view of the influence of ZPE scaling in evaluating the product ratio resulted from post-transition state bifurcation. This work will establish a basis for future QCT studies of organic reactions.

TOC GRAPHICS

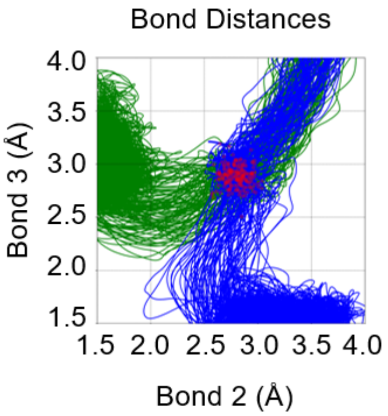

KEYWORDS

Reaction Dynamics, Bifurcation, Quasiclassical Trajectories, Zero-Point Energy, Cycloaddition, Nitrene Insertion, Nucleophilic Attack

INTRODUCTION

Post-Transition State Bifurcation (PTSB) is a phenomenon where a single ambimodal transition state leads to multiple products.[1-4] The bifurcation occurs after the transition state on the potential energy surface; this is distinct from traditional kinetically-controlled mechanisms, whose possibility for multiple products emerges from two distinct transition states with different energy barriers.[1-5] PTSB forms a new mechanistic picture for understanding outcomes in organic synthesis and has been studied for many different kinds of organic reactions, including pericyclic reactions,[6-9] nitrene insertion,[10] nucleophilic substitution,[11] ring-opening,[12,13] and rearrangement.[14-17]

Characterizing PTSB in experiments is very difficult because the higher-energy nascent product resulted from bifurcation tends to undergo a fast conversion to the most thermodynamically stable product. Accordingly, computational simulations, in particular, quasiclassical trajectories with quantum mechanical forces (QCTs), provide a key strategy to elucidate the time-resolved mechanisms for these reactions.[18-20] These trajectories are similar to traditional molecular dynamics simulations in that they use Newtonian mechanics integrated over time to predict the movements of atoms. In contrast to molecular dynamics simulations, QCTs incorporate zero-point energy to sample transition state geometries as the starting point for propagation. This treatment allows QCTs to involve quantum vibrational effects to more accurately simulate the dynamics of the reacting species. Enabled by QCT simulations, previous studies have explored the relationship between various physical factors and the resulting ratio of products or the timing of bond formation. These factors include transition structure geometries,[9,21,22] transition state momentum distribution,[3,8,23] kinetic energy distribution,[24] and condensed-media environment (e.g., solvent or enzyme)[13,25-27]. In particular, Carpenter has made ground-breaking contribution to elucidate how transition state momentum mediate bifurcation outcome, which is known as "dynamic matching" effect.

Despite the wide application of QCTs in studying PTSB, the influence of ZPE on the ratio between the products of bifurcation is not well understood. In quasiclassical dynamics, ZPE flow or leakage has been known to potentially cause artificial bonding rearrangement.[28,29] Using a fraction of ZPE can compensate for the ZPE flow/leakage problem in simple two-state systems, leading to a better reproduction of the vibrational quantum dynamics behavior.[29] However, the influence of zero-point energy on the bifurcation ratio and the timing of bond formation has not been well studied. We present an analysis of the effects of varying the percentage of the transition structure's zero-point energy used in sampling geometries on the resulting bifurcation ratio and timing associated with bond formation.

COMPUTATIONAL METHODS

Transition state structure optimization Density functional theory computations were performed using Gaussian 16.[30] The geometries of ambimodal transition state structure (TSS) and their corresponding bifurcating product ratios, either computational or experimental, were extracted from previous literature on post-TS bifurcation. The geometries collected all used B3LYP for their method but differed in the exact parameters of their basis set.[31] To ensure consistency among the trajectories propagated for this work, the structures from the literature were reoptimized using

B3LYP/6-31G(d). The coordinates for the reoptimized transition structures are shown in the Supporting Information.

Quasiclassical trajectory simulation Trajectory simulations were performed with the Progdyn/Gaussian interface developed by Singleton, as shown in Table 1.[8,32] For each of the three model reactions, quasiclassical trajectories were initialized in the vicinity of the TSS with normal-mode sampling, which involves adding zero-point energy and thermal energy for each real normal mode in the TSS and obtaining a Boltzmann distribution by randomly sampling a set of geometries and velocities. Three different percentages of the zero-point energy were used: 100% of the value present in the TSS, 50%, and 10%. No additional velocities were added other than vibrations along modes perpendicular to the reaction coordinate. The trajectories were propagated forward and backward until either one of the products is formed (defined as the forming bonds ≤ 1.6 Å) or the reactant is generated. The classical equations of motion were integrated with a velocity Verlet algorithm, with the energies and derivatives computed on the fly by the quantum mechanical method using Gaussian 16.[30] Two hundred trajectories were propagated for each of the three ZPE values for each reaction.

Table 1. The parameters used for the quasiclassical trajectory simulation.

Parameter	Value
Method/Basis Set	B3LYP/6-31G(d)
Simulation Timestep	1 fs
Simulation Length	±352 fs
Bond Length Formation Criterion	1.6 Å (C-C, C-O, C-N)
Zero-Point Energy Values	100%, 50%, 10%
Temperature	298.15 K
Software Used	Progdyn/Gaussian

RESULTS AND DISCUSSION

Reaction Selection To benchmark the effect of ZPE across different types of organic reactions, three different reactions with varying mechanisms were selected.[21,22] The two products formed (designated X and Y) for each reaction are shown in Figure 1. X is the major product in all cases. Reaction A is an intramolecular cycloaddition between a diene and a triene, where product X is a [6+4]-adduct and product Y is a [4+2]-adduct.[33] Reaction B involves intramolecular nitrene insertion into a α-fluorinated cyclohexanone, forming two different bicyclic lactams (X=9-fluoro-1-azabicyclo[4.2.1]nonan-2-one and Y=6-fluoro-1-azabicyclo[3.2.2]nonan-7-one), depending on the side of the ketone into which the nitrene is inserted.[10] Reaction C involves a nucleophilic attack from a hydroxide ion on an α-bromoketone, with product X resulting from an S_N2 reaction displacing a bromide ion and product Y resulting from the addition of the hydroxide onto the ketone, creating a deprotonated vicinal diol.[34]

The reactions differ in the number of bonds formed, type of bonds formed, and number of bonds broken. Reaction A always features the C–C bond that forms the far side of the adduct, with products X and Y arising from two different C–C bonds within the ring system. Reaction B always forms a bond between the nitrene and the carbonyl carbon, and products X and Y originate from the two C–N bonds that form as the nitrene inserts itself between one of the α-carbons and the carbonyl. This means that, in either product, one C–C bond is cleaved. In reaction C, the hydroxide may form one of two C–O bonds with either the α-carbon or the carbonyl carbon, with no bonds cleaved in either product. The differences in bond formation and cleavage across the three selected reactions offer a wider view of the effects of ZPE scaling.

These particular reactions were selected for three reasons. First, their relatively small system size (< 40 atoms) permits propagation of trajectories with a cheaper computational cost. Second, all three reactions were studied using the B3LYP level of theory and various basis sets, allowing close comparison of computational results between the original and current studies. Third, each of the reactions was reported in the previous literature not to have a symmetric bifurcation surface, suggesting that a change in ZPE likely shifts the bifurcation ratio.

Reaction	Product X	Product Y	Ratio X:Y	Method/Basis Set
A	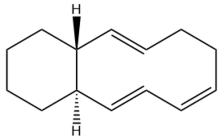	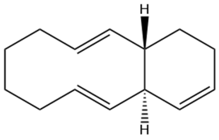	1.4:1	B3LYP/6-31G*
B	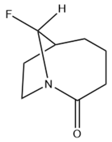	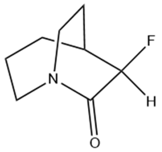	2.7:1	B3LYP/6-31+G(d,p)
C	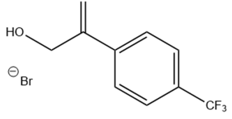	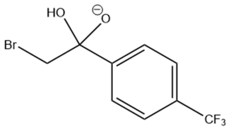	1.2:1	B3LYP/6-31+G(d)

Figure 1. Three model reactions that display post-transition state bifurcation. Reaction A is an intramolecular cycloaddition, reaction B is a nitrene insertion into a cyclic ketone, and reaction C is a nucleophilic substitution/addition. Products X and Y are used to refer to the more abundant and less abundant product between the bifurcating possibilities, respectively. The structures of products X and Y for each of the three selected reactions with their reported experimental or computational ratio and method/basis set from the literature.

Time-Resolved Mechanism for the Reactions with PTSB Quasiclassical trajectories were initiated from the optimized TSSs (Figure 2). Examining the structural changes involved in the three reactions over the course of a trajectory provides deeper insight into the specific chemistry of each reaction. Snapshots of the conversion from reactant to product in typical trajectories are shown in Figure 3. The snapshots of reaction A depict first the reactant in the reactive conformation: the diene and triene moieties must be roughly planar for the pericyclic reaction to occur. Then, bond 1 forms to close the molecule into a 14-membered ring. After that, bond 2 or 3 forms to create product X or Y, respectively. In the two typical trajectory outcomes shown in the reaction A (Figure 3), products X and Y form at 57 fs and 85 fs, respectively. Reaction B depicts the reactant's terminal methanimine group undergoing a 1,2-alkyl shift to form a nitrene that is drawn toward the ketone. A bond is formed between the nitrogen atom and the carbonyl carbon, creating a tetrahedral TSS. After this TS, the nitrene inserts itself into one of the bonds between the carbonyl carbon and an α-carbons, simultaneously creating a C–N bond (bond 2 or 3) and cleaving a C–C bond. By inserting a bridging nitrogen into either side of a cyclohexanone, either a [4.2.1] or a [3.2.2] bicyclic product can be created. The two trajectories shown in the reaction B (Figure 3) form products X and Y at 71 fs and 123 fs, respectively. Reaction C displays relatively simple nucleophilic chemistry, where hydroxide ion could attack either of the two electrophilic sites. Both the carbonyl carbon and the α-carbon are electron-deficient from the inductive effects of the oxygen and bromine, respectively, and thus attract the electron-rich hydroxide ion. As the hydroxide ion approaches the α-carbon, the C–Br bond lengthens until the bromide dissociates entirely. When the hydroxide attacks and opens the ketone, a rearrangement is observed to form a tetrahedral structure from the trigonal planar ketone. In the reaction C (Figure 3), product X forms at 69 fs and product Y forms at 140 fs.

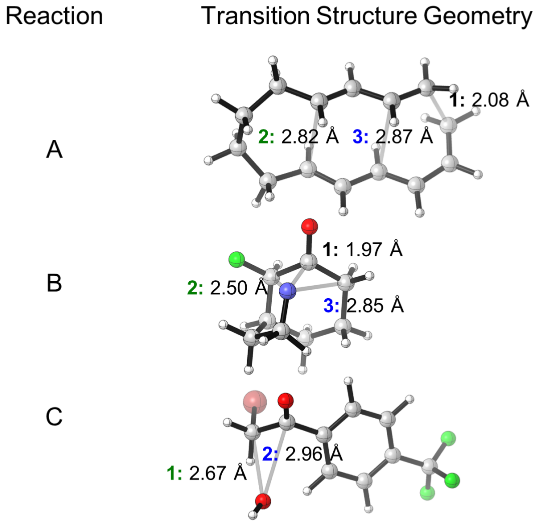

Figure 2. The optimized TSSs for the model reactions. Bonds whose formation leads to product X (bond 2 for reactions A and B, bond 1 for reaction C) are labeled in green, while the bonds responsible for product Y (bond 3 for reactions A and B, bond 2 for reaction C) are labeled in blue.

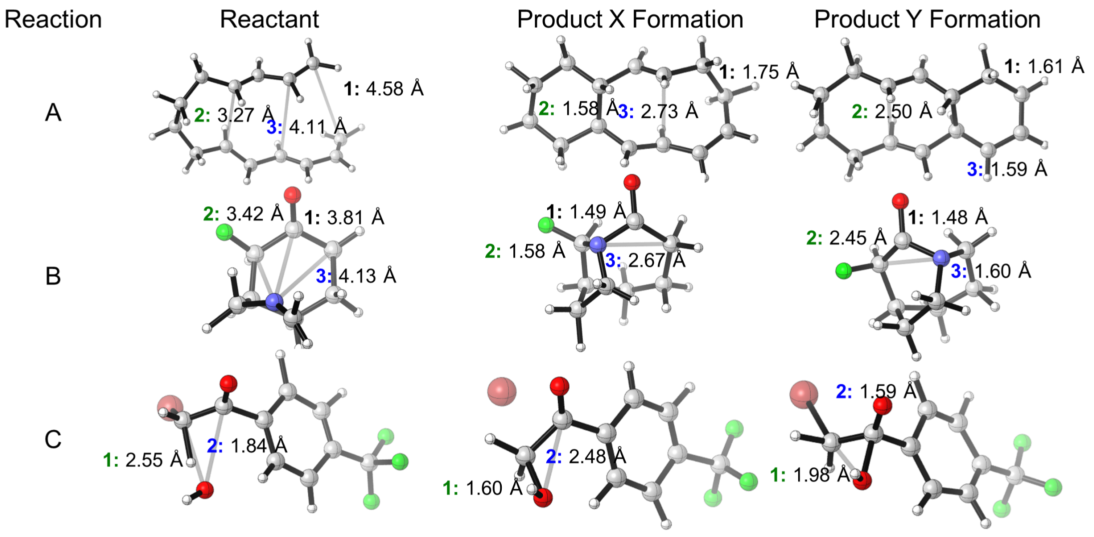

Figure 3. Snapshots from two typical trajectories for each of the three reactions at different points in their progression from reactant to product. The reactant snapshot was taken at 100 fs prior to the transition structure geometry in the trajectory that forms product X, while the product snapshots are from the point of trajectories that lead to product X formation or product Y formation, respectively. Product formation is defined as when the last forming bond becomes ≤1.6 Å. Bonds whose formation leads to product X (bond 2 for reactions A and B, bond 1 for reaction C) are labeled in green, while the bonds responsible for product Y (bond 3 for reactions A and B, bond 2 for reaction C) are labeled in blue.

The Impact of ZPE Percentage on the Bifurcation Ratio Across the selected model reactions, the ratio of product X: product Y was computed for the productive trajectories. The results for each of the three ZPE percentages used are summarized in Figure 4. For reaction A, there is only a very slight trend in the ratio across the three values, and the ratio decreases with ZPE, going from 1.5:1 at 100% to 1.4:1 at 10%. Reaction B shows a much greater trend, increasing from 5.3:1 at 100% ZPE to 8.3:1 at 10% ZPE. Reaction C shows a distinct, though less intense trend, increasing from 4.8:1 at 100% to 6.5:1 at 10%. The plots shown display the bifurcation via coloring of trajectories based on the product formed. These results show that reaction B is most sensitive to the variation of ZPE percentage, reaction C is moderately sensitive, and reaction A is insensitive.

Notably, the sensitivity of the reaction to the ZPE percentage is correlated to the bond length difference (i.e., asyncronicity) between the two competing bonds (i.e., bond 2 and 3) in the TSS (Figure 2). The difference is large for the reaction B (i.e., bond 2 is 0.35 Å shorter than bond 3), moderate for the reaction C (i.e., bond 1 is 0.29 Å shorter than bond 2), and very small for the reaction A (i.e., bond 2 is 0.05 Å shorter than bond 3). We hypothesize that, for reactions B and C, the dynamic formation of the minor product is promoted by the correlated motion that brings together the atoms which compose the bond leading to product Y. The coupled motion is associated with a certain vibrational mode that represent the breathing or wagging motion of the molecular scaffold. Decreasing the ZPE fraction reduces the momentum for the correlated motion, causing more of the trajectories to go toward the more favored product. For reaction A, this smaller difference results in little change in the ratio.

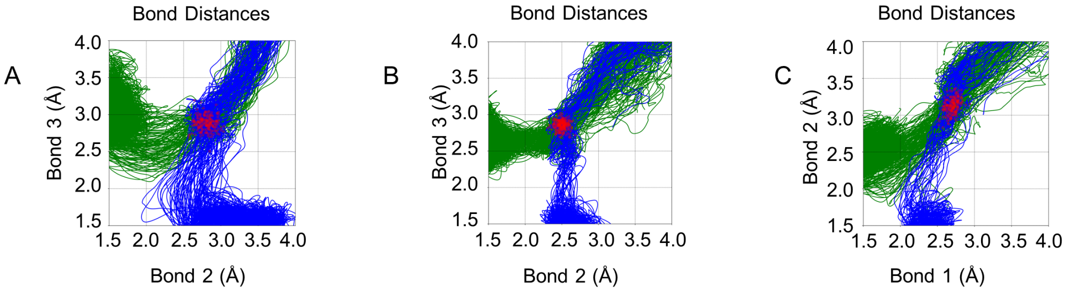

ZPE	Product X:Y
100%	1.5:1
50%	1.5:1
10%	1.4:1

ZPE	Product X:Y
100%	5.3:1
50%	5.8:1
10%	8.3:1

ZPE	Product X:Y
100%	4.8:1
50%	5.0:1
10%	6.5:1

Figure 4. Post-TS bifurcation ratios for the three reaction. The plots showing the bond lengths corresponding to products X and Y for the three selected reactions depict the trajectories

collected with 100% ZPE. Trajectories leading to X are shown in green while those leading to Y are shown in blue. The red circles indicate the bond lengths at the transition structures from which the trajectories were propagated. The tables below show the product X:Y ratio for the three reactions at each of the three ZPE values.

Bond Formation Time Analysis The gap between the formation of the shared bond (1) and either of the two-product specific bonds (2 & 3) can inform analyses of the resulting product ratio. For reaction A, the median bond formation time gap for productive trajectories increased for product X and decreased for product Y as ZPE percentage decreased, as show in Figure 5; this is consistent with a slight decrease in the X:Y ratio discussed above. As X takes more time to form and Y takes less, it becomes more likely that product Y will form. Reaction B shows the opposite trend, with product X's time gap decreasing slightly while that for Y increases. This is also consistent with an increase in the X:Y ratio, reflecting the increased difficulty of forming bond 3 upon the reduction of momentum for the coupled motion. For reaction C, time gap cannot be consistently assessed, as there is no bond that is formed in common between the two products. Accordingly, the time of formation for bonds 1 and 2 (forming products X and Y respectively) after the TS is used instead. Reaction C follows a similar trend to reaction B. A decrease in ZPE is correlated with faster formation of product X and slower formation of product Y, which is consistent with the ratio changes discussed previously.

These data support the hypothesis presented above. As less ZPE is put into the system, there is less momentum for the global vibrational motion to overcome greater distance between the transition state and product Y's geometry. This is reflected in the larger amount of time needed to form product Y and correspondingly a decrease in its prevalence among the trajectories. A greater ratio between the products at 100% ZPE also indicates that the geometric difference between the products is greater, meaning that a decrease in ZPE would more significantly affect the forming trajectories. This could explain the trend seen in A’s ratio changing only slightly, while that for B changes more.

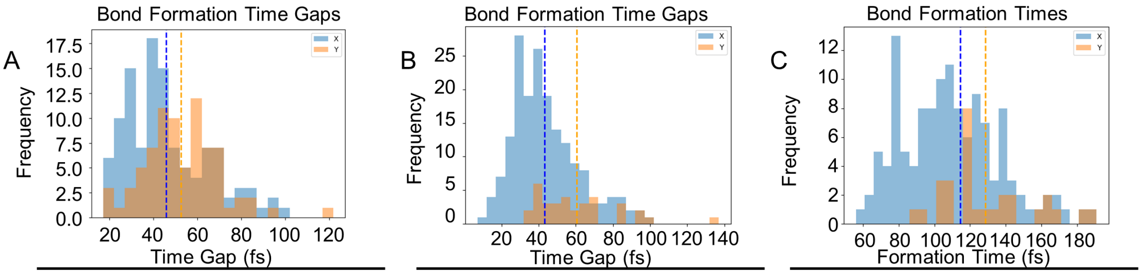

ZPE	Product X	Product Y
100%	42 fs	51 fs
50%	44 fs	46 fs
10%	47 fs	48 fs

ZPE	Product X	Product Y
100%	39 fs	55.5 fs
50%	39 fs	56 fs
10%	37 fs	62 fs

ZPE	Product X	Product Y
100%	108 fs	119 fs
50%	105 fs	129 fs
10%	102 fs	126 fs

Figure 5. Information regarding the distributions of bond formation time gaps (for reactions A and B) or times post-TS (for reaction C) The histograms depict the distributions for the three reactions at 100% of the zero-point energy. The vertical line indicates the mean value of the distribution. The tables below show the median times for the three reactions at each of the three ZPE values.

Analysis of Dynamically-Concerted vs Stepwise Trajectories For reactions A and B, the percentage of trajectories that formed product X categorized as dynamically-concerted[35] (bond formation gap < 60 fs, the lifetime of a transition state) was computed. Those forming product Y were not characterized since it is the minor product for the reactions and would not provide enough data from which to draw conclusions. Reaction C involves a distinct mode of bond rearrangement from Reaction A or B, and is thus not taken into comparison. Reaction A shows an overall increase in the percentage of concerted mechanisms as the zero-point energy decreases, though the trend is unsteady. In contrast, reaction B shows a steady increase in concerted trajectories as ZPE decreases.

When the reactants have greater zero-point energy, the global vibrational motion is more energized, leading to a competition between formation of bonds. The competition elongates the lifetime of dynamic intermediates before they form the products. However, as ZPE decreases, there is less energy available to promote the coupled motion that is essential for the formation of the minor product. Accordingly, there is a decrease in the percentage of dynamically-stepwise mechanisms.

Table 2. The percentage of trajectories leading to product X categorized as dynamically-concerted (bond formation gap < 60 fs, the lifetime of a transition state) for reactions A and B. Since reaction C possesses a one-step mechanism, it cannot be categorized as stepwise or concerted.

Reaction	ZPE Percentage	% Dynamically-Concerted
A	100	76.1
	50	80.3
	10	79.3
B	100	83.2
	50	84.6
	10	90.3

CONCLUSION

We have examined three different bifurcating organic reactions and benchmarked the effect of altering the zero-point energy percentage used in simulating reaction trajectories for each in terms of the resulting bifurcation ratio and timing associated with bond-formation. As the ZPE percentage decreases, the ratio trends toward the major product, with the intensity of that trend dictated by the difference of lengths of the forming bonds within the transition structure. We hypothesize that this is due to a decrease in momentum for correlated motion as the ZPE decreases which prevents the atoms whose bond leads to the minor product from being brought together, thus promoting formation of the more favored major product.

ASSOCIATED CONTENT

Supporting Information. Cartesian coordinates of the optimized transition structures (PDF)

AUTHOR INFORMATION

Corresponding Author

*email: zhongyue.yang@vanderbilt.edu phone: 615-343-9849

Notes

The authors declare no competing financial interest.

ACKNOWLEDGMENT

This research was supported by a startup grant from Vanderbilt University and a scholarship from the Vanderbilt Institue of Chemical Biology. This work was carried out in part using computational resources from the Extreme Science and Engineering Discovery Environment (XSEDE) which is supported by National Science Foundation grant number TG-BIO200057.[36]

REFERENCES

1 Ess, D. H. *et al*. Bifurcations on Potential Energy Surfaces of Organic Reactions. *Angewandte Chemie International Edition* **47**, 7592-7601, doi:10.1002/anie.200800918 (2008).

2 Hare, S. R. & Tantillo, D. J. Post-transition state bifurcations gain momentum – current state of the field. *Pure and Applied Chemistry* **89**, 679-698, doi:10.1515/pac-2017-0104 (2017).

3 Rehbein, J. & Carpenter, B. K. Do we fully understand what controls chemical selectivity? *Physical Chemistry Chemical Physics* **13**, 20906, doi:10.1039/c1cp22565k (2011).

4 Chuang, H.-H., Tantillo, D. J. & Hsu, C.-P. Construction of Two-Dimensional Potential Energy Surfaces of Reactions with Post-Transition-State Bifurcations. *Journal of Chemical Theory and Computation* **16**, 4050-4060, doi:10.1021/acs.jctc.0c00172 (2020).

5 Carpenter, B. K. Dynamic Behavior of Organic Reactive Intermediates. *Angewandte Chemie International Edition* **37**, 3340-3350, doi:https://doi.org/10.1002/(SICI)1521-3773(19981231)37:24<3340::AID-ANIE3340>3.0.CO;2-1 (1998).

6 Xue, X.-S. *et al*. Ambimodal Trispericyclic Transition State and Dynamic Control of Periselectivity. *Journal of the American Chemical Society* **141**, 1217-1221, doi:10.1021/jacs.8b12674 (2019).

7 Jamieson, C. S., Ohashi, M., Liu, F., Tang, Y. & Houk, K. N. The expanding world of biosynthetic pericyclases: cooperation of experiment and theory for discovery. *Natural Product Reports* **36**, 698-713, doi:10.1039/c8np00075a (2019).

8 Wang, Z., Hirschi, J. S. & Singleton, D. A. Recrossing and Dynamic Matching Effects on Selectivity in a Diels–Alder Reaction. *Angewandte Chemie* **121**, 9320-9323, doi:10.1002/ANGE.200903293 (2009).

9 Thomas, J. B., Waas, J. R., Harmata, M. & Singleton, D. A. Control Elements in Dynamically Determined Selectivity on a Bifurcating Surface. *Journal of the American Chemical Society* **130**, 14544-14555, doi:10.1021/ja802577v (2008).

10 Campos, R. B., Tantillo, D. J. & Tantillo, C. Designing Reactions with Post-Transition-State Bifurcations: Asynchronous Nitrene Insertions into C-C s Bonds HIGHLIGHTS A recipe for designing reactions with post-transition-state bifurcations is provided A model for selectivity control for such reactions is presented Designing Reactions with Post-Transition-State Bifurcations: Asynchronous Nitrene Insertions into C-C s Bonds. *Chem* **5**, 227-236, doi:10.1016/j.chempr.2018.10.019 (2018).

11 Bogle, X. S. & Singleton, D. A. Dynamic Origin of the Stereoselectivity of a Nucleophilic Substitution Reaction. *Organic Letters* **14**, 2528-2531, doi:10.1021/ol300817a (2012).

12 Kramer, Z. C., Carpenter, B. K., Ezra, G. S. & Wiggins, S. Reaction Path Bifurcation in an Electrocyclic Reaction: Ring-Opening of the Cyclopropyl Radical. *The Journal of Physical Chemistry A* **119**, 6611-6630, doi:10.1021/acs.jpca.5b02834 (2015).

13 Carpenter, B. K., Harvey, J. N. & Glowacki, D. R. Prediction of enhanced solvent-induced enantioselectivity for a ring opening with a bifurcating reaction path. *Physical Chemistry Chemical Physics* **17**, 8372-8381, doi:10.1039/c4cp05078a (2015).

14 Siebert, M. R., Manikandan, P., Sun, R., Tantillo, D. J. & Hase, W. L. Gas-Phase Chemical Dynamics Simulations on the Bifurcating Pathway of the Pimaradienyl Cation Rearrangement: Role of Enzymatic Steering in Abietic Acid Biosynthesis. *Journal of Chemical Theory and Computation* **8**, 1212-1222, doi:10.1021/ct300037p (2012).

15 Yamataka, H., Sato, M., Hasegawa, H. & Ammal, S. C. Dynamic path bifurcation for the Beckmann reaction: observation and implication. *Faraday Discuss.* **145**, 327-340, doi:10.1039/b906159b (2010).

16 Hrovat, D. A., Fang, S., Borden, W. T. & Carpenter, B. K. Investigation of Cyclopropane Stereomutation by Quasiclassical Trajectories on an Analytical Potential Energy Surface. *Journal of the American Chemical Society* **119**, 5253-5254, doi:10.1021/ja964238s (1997).

17 Newman-Evans, R. H., Simon, R. J. & Carpenter, B. K. The influence of intramolecular dynamics on branching ratios in thermal rearrangements. *The Journal of Organic Chemistry* **55**, 695-711, doi:10.1021/jo00289a053 (1990).

18 Doubleday, C., Bolton, K. & Hase, W. L. Direct Dynamics Quasiclassical Trajectory Study of the Thermal Stereomutations of Cyclopropane. *The Journal of Physical Chemistry A* **102**, 3648-3658, doi:10.1021/jp973273y (1998).

19 Paranjothy, M., Sun, R., Zhuang, Y. & Hase, W. L. Direct chemical dynamics simulations: coupling of classical and quasiclassical trajectories with electronic structure theory. *WIREs Computational Molecular Science* **3**, 296-316, doi:https://doi.org/10.1002/wcms.1132 (2013).

20 Sun, L. & Hase, W. L. Comparisons of classical and Wigner sampling of transition state energy levels for quasiclassical trajectory chemical dynamics simulations. *The Journal of Chemical Physics* **133**, 044313, doi:10.1063/1.3463717 (2010).

21 Yang, Z. *et al*. Relationships between Product Ratios in Ambimodal Pericyclic Reactions and Bond Lengths in Transition Structures. *Journal of the American Chemical Society* **140**, 3061-3067, doi:10.1021/JACS.7B13562 (2018).

22 Lee, S. & Goodman, J. M. Rapid Route-Finding for Bifurcating Organic Reactions. *Journal of the American Chemical Society* **142**, 9210-9219, doi:10.1021/JACS.9B13449 (2020).

23 Ussing, B. R., Hang, C. & Singleton, D. A. Dynamic Effects on the Periselectivity, Rate, Isotope Effects, and Mechanism of Cycloadditions of Ketenes with Cyclopentadiene. *Journal of the American Chemical Society* **128**, 7594-7607, doi:10.1021/ja0606024 (2006).

24 Bharadwaz, P., Maldonado-Domínguez, M. & Srnec, M. Bifurcating reactions: distribution of products from energy distribution in a shared reactive mode. *Chemical Science* **12**, 12682-12694, doi:10.1039/D1SC02826J (2021).

25 Yang, Z. *et al*. Influence of water and enzyme SpnF on the dynamics and energetics of the ambimodal [6+4]/[4+2] cycloaddition. *Proceedings of the National Academy of Sciences* **115**, E848-E855, doi:10.1073/pnas.1719368115 (2018).

26 Chen, Z., Nieves-Quinones, Y., Waas, J. R. & Singleton, D. A. Isotope Effects, Dynamic Matching, and Solvent Dynamics in a Wittig Reaction. Betaines as Bypassed Intermediates. *Journal of the American Chemical Society* **136**, 13122-13125, doi:10.1021/ja506497b (2014).

27 Siebert, M. R., Zhang, J., Addepalli, S. V., Tantillo, D. J. & Hase, W. L. The Need for Enzymatic Steering in Abietic Acid Biosynthesis: Gas-Phase Chemical Dynamics Simulations of Carbocation Rearrangements on a Bifurcating Potential Energy Surface. *Journal of the American Chemical Society* **133**, 8335-8343, doi:10.1021/ja201730y (2011).

28 Doubleday, C., Boguslav, M., Howell, C., Korotkin, S. D. & Shaked, D. Trajectory Calculations for Bergman Cyclization Predict H/D Kinetic Isotope Effects Due to Nonstatistical Dynamics in the Product. *Journal of the American Chemical Society* **138**, 7476-7479, doi:10.1021/jacs.6b03466 (2016).

29 Müller, U. & Stock, G. Flow of zero-point energy and exploration of phase space in classical simulations of quantum relaxation dynamics. II. Application to nonadiabatic processes. *The Journal of Chemical Physics* **111**, 77-88, doi:10.1063/1.479255 (1999).

30 Gaussian 16, Revision B.01 (Gaussian, Inc., Wallingford CT, 2016).

31 Lee, C., Yang, W. & Parr, R. G. Development of the Colle-Salvetti correlation-energy formula into a functional of the electron density. *Physical Review B* **37**, 785-789, doi:10.1103/physrevb.37.785 (1988).

32 Kelly, K. K., Hirschi, J. S. & Singleton, D. A. Newtonian Kinetic Isotope Effects. Observation, Prediction, and Origin of Heavy-Atom Dynamic Isotope Effects. *Journal of the American Chemical Society* **131**, 8382-8383, doi:10.1021/ja9031083 (2009).

33 Zhang, B. *et al*. Enzyme-catalysed [6+4] cycloadditions in the biosynthesis of natural products. *Nature* **568**, 122-126, doi:10.1038/s41586-019-1021-x (2019).

34 Itoh, S., Yoshimura, N., Sato, M. & Yamataka, H. Computational Study on the Reaction Pathway of α-Bromoacetophenones with Hydroxide Ion: Possible Path Bifurcation in the Addition/Substitution Mechanism. *The Journal of Organic Chemistry* **76**, 8294-8299, doi:10.1021/jo201485y (2011).

35 Yang, Z. *et al*. Molecular dynamics of the two-stage mechanism of cyclopentadiene dimerization: concerted or stepwise? *Chemical Physics* **514**, 120-125, doi:10.1016/J.CHEMPHYS.2018.02.020 (2018).

36 Towns, J. *et al*. XSEDE: Accelerating Scientific Discovery. *Computing in Science & Engineering* **16**, 62-74, doi:10.1109/MCSE.2014.80 (2014).